Clay Minerals, (2015) **50**, 583–592

The formation of a hydrotalcite coating on the aluminium alloy 6060 using a spray system

LINGLI ZHOU[1,2,*], HENRIK FRIIS[1], MELANIE ROEFZAAD[3], KASPER BONDO HANSEN[3], SARA EISENHARDT[3], ASGER ANDERSEN[3] AND NIKOLAJ ZANGENBERG[4]

[1] *Department of Geoscience, Aarhus University, Høegh-Guldbergs Gade 2, DK-8000 Aarhus C, Denmark*
[2] *Key Laboratory of Mineral Resources, Institute of Geology and Geophysics, Chinese Academy of Sciences, 19 Beituchen Western Road, Chaoyang District, Beijing 100029, China*
[3] *Siemens Corporate Technology, Borupvang 9, 2750 Ballerup, Denmark*
[4] *Danish Technological Institute, Kongsvang Allé 29, 8000 Aarhus C, Denmark*

(*Received 1 December 2014; revised 3 September 2015; Associate Editor: Helge Stanjek*)

ABSTRACT: Coatings with the composition of Li-Al-NO_3 hydrotalcite were formed on the Al alloy 6060 using a spray system. The coatings consist of crystals with a typical hydrotalcite structure. Dense, uniform and blade-like flakes cover completely the surface of the Al substrate. The coatings display a multi-layer structure with average thickness of ~1000 nm. The hydrotalcite-coated samples performed better than those without coatings in salt-spray and filiform-corrosion tests, and further treatment involving sealing with a Mg acetate solution and dipping in a H_2O_2 + Ce-based solution improved the corrosion resistance ability.

KEYWORDS: Al alloy 6060, hydrotalcite, coating, spray system.

INTRODUCTION

Hydrotalcite is a hydroxycarbonate of magnesium and aluminium occurring in nature as foliated and contorted plates and/or fibrous masses. Fundamentally, it is an anionic clay with layered double hydroxides. A general formula for hydrotalcite-like compounds is: $[M^{2+}_{1-x}M^{3+}_{x}(OH)_2]^{x+}(A^{n-}_{x/n})\cdot mH_2O$, where M^{2+} and M^{3+} represent the divalent and trivalent cations, respectively, A^{n-} is the interlayer anion which is replaceable by other anions and n is the charge of the interlayer anion, x is the $M^{3+}/(M^{2+}+M^{3+})$ mol ratio and m is the number of associated water molecules (Cavani *et al*., 1991). For the purposes of the present study, hydrotalcite was taken as a reference name for its isomorphous and polytype compounds.

Many practical applications have been found for the anionic clays based on hydrotalcite-like compounds (Taylor, 1984; Reichle, 1986; Cavani *et al*., 1991; Basile & Vaccari, 2001; Orthman *et al*., 2003; Kannan, 2006). In corrosion research, hydrotalcite-like compounds acting as anti-corrosive inhibitors loaded with different anions have attracted increasing attention as possible replacements of Cr-based conversion coatings (Buchheit *et al*., 2002, 2003; Zhang & Buchheit, 2002; Williams & McMurray, 2003, 2004; Lin *et al*., 2007; Wang *et al*., 2010). The corrosion-inhibiting properties of different types of coatings (conversion coating, sol-gels, model coatings, commercial primers, *etc*.) formulated with various hydrotalcite-like compounds have been assessed (Lin & Uan, 2009; Chen *et al*., 2012; Syu *et al*., 2013) and

*Email: lingli.zhou@geo.au.dk
DOI: 10.1180/claymin.2015.050.5.03

improvements in anti-corrosive hydrotalcite-conversion coatings on AZ91D alloy (Wang *et al*., 2010; Chen *et al*., 2012), AA2024 alloy (Buchheit *et al*., 2002; Williams & McMurray, 2003), Al 6061 alloy (Valdez *et al*., 2014) and galvanized steel (Buchheit & Guan, 2004) have been proposed and evaluated. Most of these laboratory studies were carried out by dipping the panels into solutions or hanging them in autoclaves, however, methods which impose significant limits on the industrial applications of hydrotalcite coatings. Quick and spontaneous formation of coating (Li-Al-NO_3 hydroxide compounds) on the Al 6060 alloy in a spray system is described here.

EXPERIMENTAL

Formation of the hydrotalcite coating

Rectangular aluminium 6060 sheets (150 mm × 50 mm) of aluminium alloy from Siemens (Germany) were employed as substrates upon which hydrotalcite coating was deposited. Prior to spray coating, the substrate surface was etched with NaOH and HNO_3 and rinsed with water in between and afterwards. The coating solution contains a mixture of lithium, potassium and sodium salts, and the mixed solution was injected into the spray system and carried by high-temperature steam to react with the substrate to form a coating layer on the surface. A detailed description of the composition of the coating solution was given by Buchheit *et al*. (2002). The Al alloy coated with hydrotaclite and without any other, subsequent treatment was named Sample 2, and two small panels cut from different areas on Sample 2 are referred to hereafter as Sample 2-1 and Sample 2-2, respectively. Sample 4 is the hydrotalcite-coated Al alloy that was rinsed with magnesium acetate solution ($Mg(CH_3COO)_2$) for subsequent pore sealing. Immersion of the panel into a H_2O_2 + Ce-based solution was applied for further sealing, and the panel was named Sample 5.

Characterization techniques

The coating morphology was studied by Scanning Electron Microscopy (SEM) using an FEI Quanta 200 ESEM FEG instrument at the Center for Electron Nanoscopy, Technical University of Denmark, with a field-emission gun operated at 20 kV. The electron signal was detected by the in-lens detection system. Depth profiling analyses of the coated samples were carried out using Glow Discharge Optical Emission (GDOES) at the Technical University of Denmark. The GDOES was performed using a Join Yvonne RF GD-Profiler instrument equipped with a 2-mm diameter anode, operated at room temperature with a typical radio frequency discharge pressure of 850 Pa and power of 40 W. The setup was calibrated using standard materials of known compositions. The identification of the mineral types and their structure on the coating was performed by X-ray diffraction (XRD) at Aarhus University. The instrument is a Panalytical X'pert Pro with an incident-beam monochromator of germanium. It has an X-ray source of CuKα, with $\lambda = 1.5406$ Å and a secondary monochromator of graphite. Step heating (step size of 50°C, over the range 0 to 400°C) coupled with XRD was further performed using the same instrument on the same batch of samples to confirm the mineralogical compositions.

Corrosion-resistance tests

The corrosion resistance ability of coatings was evaluated using Electrochemical Impedance Spectroscopy (EIS) at Technical University of Denmark. Paints with the same treatment (not the same batch as for the EIS test) were subjected to the filiform-corrosion test by exposure to oxygen, aggressive anions (Cl^-) and a relative humidity of 60–95% (Ruggieri & Beck, 1983). The results of filiform-corrosion testing for 1000 h, in accordance with test method DIN EN 3665, are comparable with those of ~10 y of Hoek van Holland weathering (GSB International Info Letter No. 7). For electrochemical impedance measurements a two-electrode set-up, with 0.5 M NaCl as the electrolyte, was used. The measurements were performed at open-circuit potential with an AC voltage of 10 mV in the frequency range of 0.1 MHz to 50 mHz. Before each measurement, stabilization of Oxide Characteristics and Speciation (OCP) was awaited for at least 30 min. The filiform corrosion test was run for 1000 h. Standard DIN EN 3665(08.97) was applied to evaluate the test results.

RESULTS

Morphology of the coating

Representative SEM images of the coatings formed on Al 6060 alloy are shown in Fig. 1a–d. The coatings consisted of a mass of intersecting platy crystals with crystal edges pointing outwards (Fig. 1a,c). In all cases, a compact and smooth film, white to grey in colour, was noted (Fig. 1b,d). The platy crystals grew perpendicular to the alloy surface, and this "standing"

https://doi.org/10.1180/claymin.2015.050.5.03 Published online by Cambridge University Press

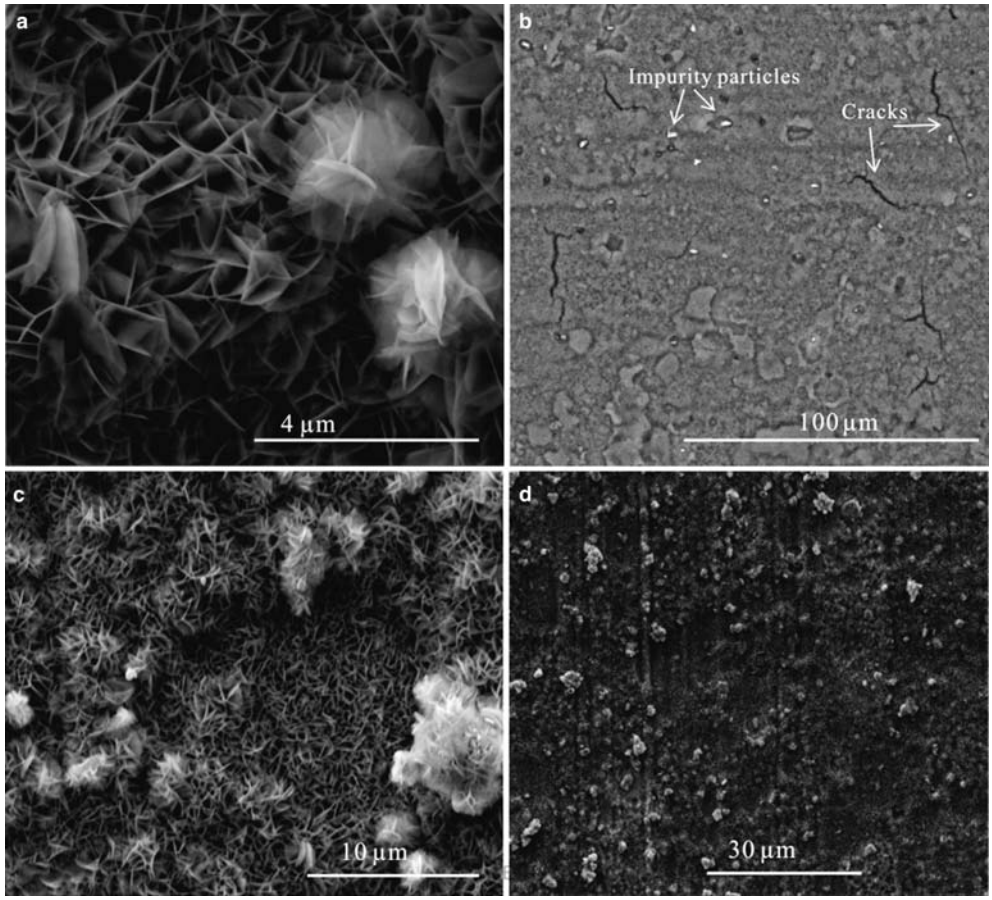

FIG. 1. SEM images of the morphology of hydrotalcite coating, sample 2.

growth pattern can be attributed to crystal growth at the edges, and the crystal nuclei with edges pointing outwards can lead to reactant species in solution more easily. Particle craters were also observed in the coatings and cracks were visible locally on the surface (Fig. 1b).

Mineralogical composition of the coating

To confirm the mineralogical composition and structure of the coatings, a slice of coated Al-plate was prepared for analysis by X-ray diffraction (XRD). The major peaks identified in the XRD patterns are from the basal Al substrate, and among the other peaks, general features of hydrotalcite compounds (Valente *et al*., 2012) were detected. Diffraction from the hydroxide layers ([003] planes) of Li-Al-NO_3 hydrotalcite ($Li_2Al_4(NO_3)_2(OH)_{12}\cdot 3H_2O$) leads to the most intense peaks in the patterns ($d = 7.59$ Å), followed by [006] planes ($d = 3.97$ Å, Fig. 2). Minor Al_2O_3 is also present in the coatings (Fig. 2). One small peak with $d = 3.95$ Å appears in all the XRD analyses, possibly as a result of MnO_2 particles in the alloy (Fig. 2). In sample 4, the presence of two new sharp reflections may be due to the occurrence of a new phase of Mg-Al-CO_3 hydrotalcite ($MgAl_4CO_3(OH)_{12}$, $d = 11.18$ Å, 5.63 Å). Similar d spacing values were observed in the XRD pattern of hydrated M(II)M(III)SO_4 hydrotalcite ($d = 11.15$ Å, 5.50 Å, Brindley & Kikkawa, 1980). In the experiments described, the replacement of NO_3^- and Li^+ by CO_3^{2-} and Mg^{2+}, leading to the formation of Mg-Al-CO_3 hydrotalcite, is possible as a result of the exposure of Li-Al-NO_3 hydrotalcite coating to Mg acetate in a subsequent sealing process.

During the step heating, one major peak ($d =$ 7.59 Å) from Li-Al-NO_3 hydrotalcite disappeared at

https://doi.org/10.1180/claymin.2015.050.5.03 Published online by Cambridge University Press

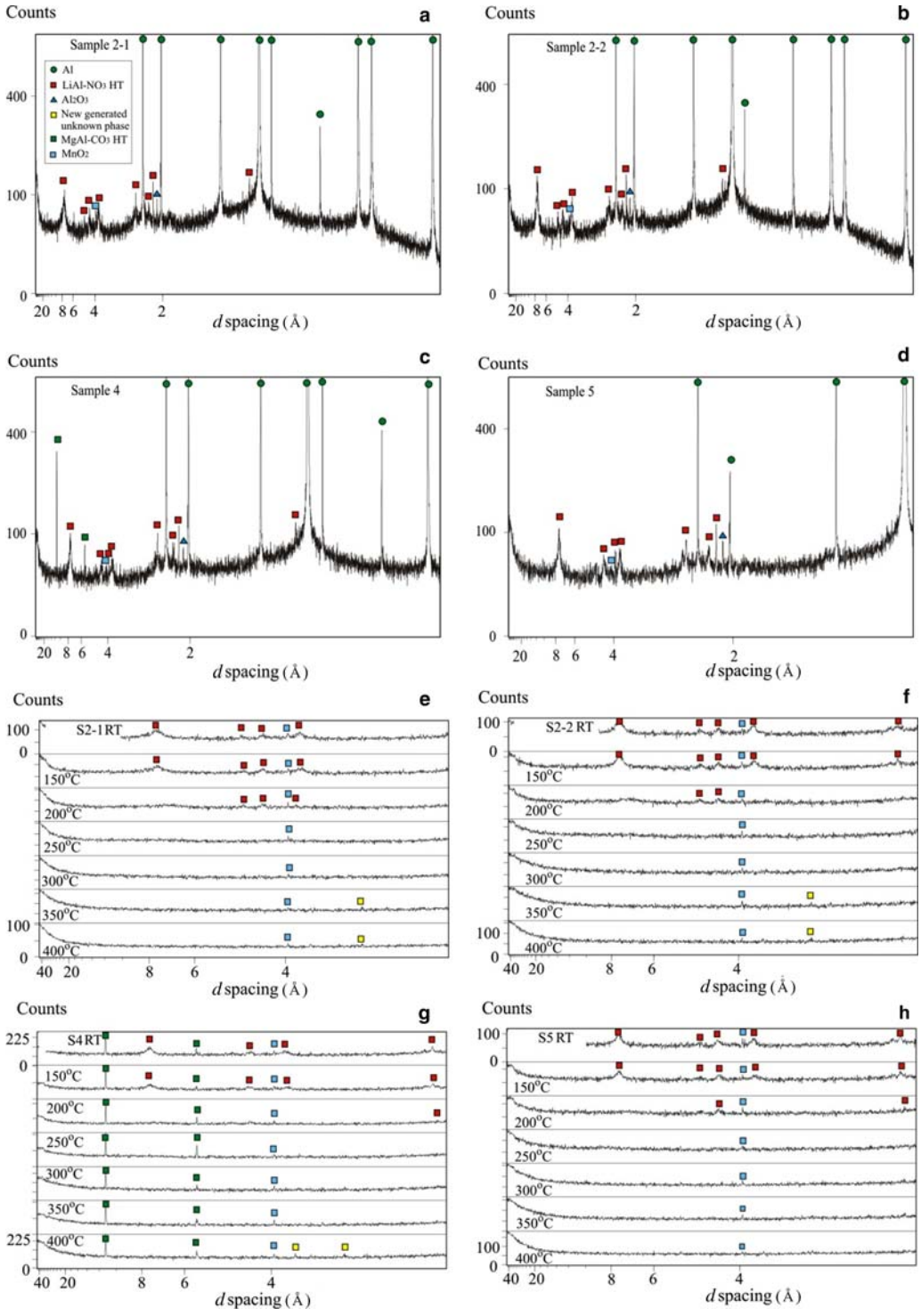

FIG 2. XRD patterns of samples with hydrotalcite coating. RT: room temperature.

https://doi.org/10.1180/claymin.2015.050.5.03 Published online by Cambridge University Press

a temperature between 150 and 200°C for all the samples (Fig. 2e–h), which may relate to the dehydration of layers in the crystal structure of Li-Al-NO_3 hydrotalcite. The interlayer structure of Li-Al-NO_3 hydrotalcite began to decompose as the temperature increased to 200–250°C, corresponding to the continuous disappearance of XRD peaks at $d = 4.36$, 3.97, 3.78 and 2.49 Å. In contrast, the Mg-Al-CO_3 hydrotalcite was thermally stable over a wide range of temperatures (Fig. 2g, room temperature, RT to 400°C), due to the strong affinity of CO_3^{2-}. Similar thermal behaviour was reported for both the synthetic and natural Mg-Al-CO_3 hydrotalcites (Valente *et al*., 2012). An unknown phase with $d = 3.34$ Å was developed at $T = 350$°C during the step heating of the samples (Fig. 2e–h).

Depth profiling of the coating

The counts of selected elements *vs.* time, obtained from the GDOES analysis, are shown in Fig. 3. The profiles of different elements stabilized since $T = 32$ s, and the profile data collected afterwards were expected to be from the basal Al substrate. The depth corresponding to $T = 32$ s may represent the approximate coating thickness, and the four coated samples give quite consistent results with respect to the coating thickness of ~1000 nm (Fig. 3). The changing tendency of Li content in the profile suggests not only the involvement of Li in the coating, but also a layered structure of the coating (Fig. 3). Before the peak point in the Li profile, the Li content increases with the Al content, whereas, after this point, the Li and Al contents were negatively correlated. Because the GDOES measurements were performed at room temperature, the Li ion can be very diffusive and penetrate the coating layer. The maxima of the Li profile may therefore represent a maximum enrichment of the Li ion at the layer interface due to a reduced mobility (Barisone *et al*., 2011). A change in diffusion velocity of Li hints at a layered structure of the coating formed. The fluctuations at $T = 30$ s in samples 2-1 and 2-2 may suggest a non-continuous and heterogeneous coating. The preference for crystals to 'stand' on the coatings leaves micro-pores within the stacks of layers (Fig. 1a,c), reducing the Li signals and giving rise to the fluctuations in the Li profile (Fig. 3).

A multi-layer structure was confirmed by the cross-sectional morphology observed in the FIB-SEM analysis. At least two layers are present in the coatings

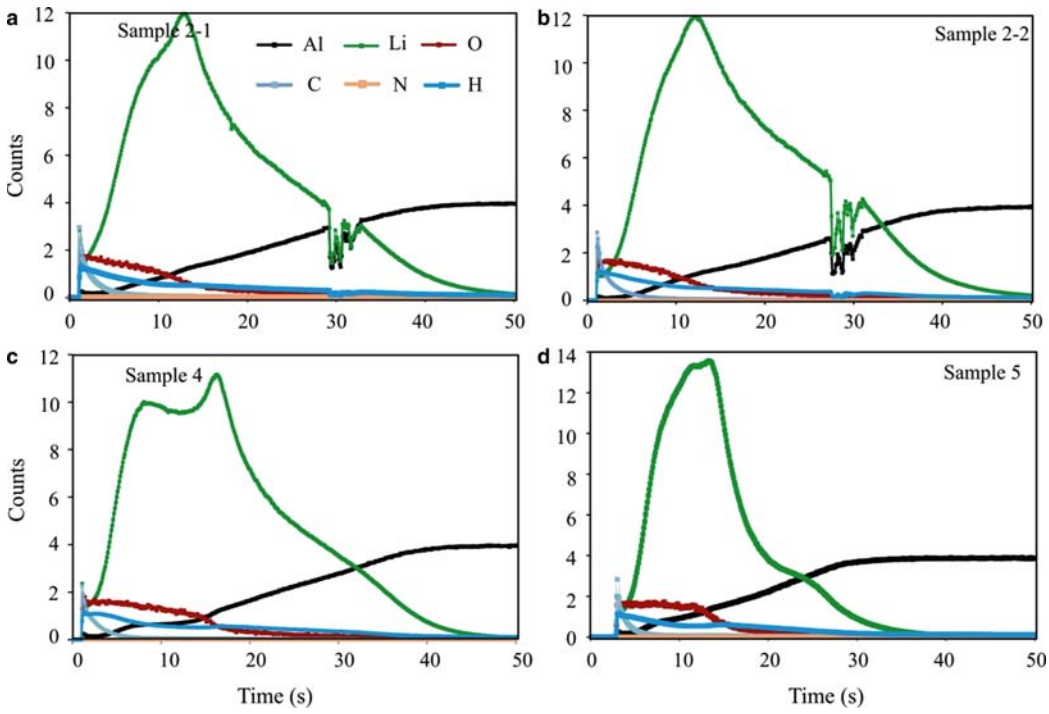

FIG 3. GDOES results of the depth profile of hydrotalcite coatings.

https://doi.org/10.1180/claymin.2015.050.5.03 Published online by Cambridge University Press

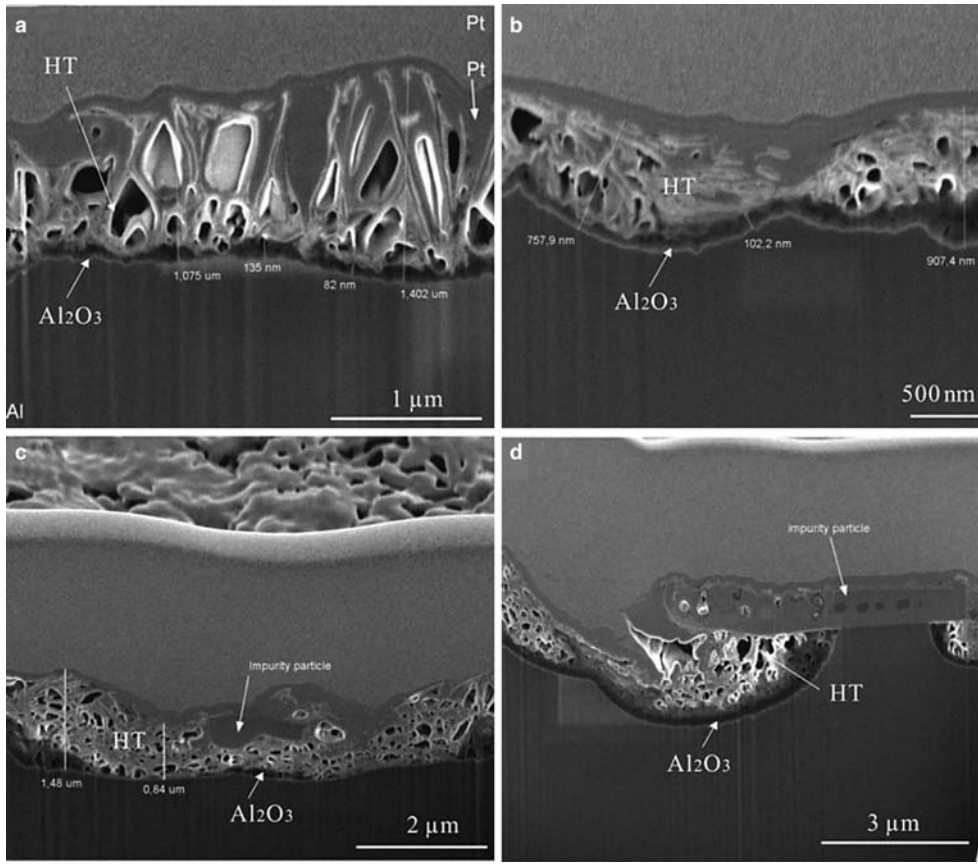

FIG 4. Cross-sectional morphologies of the samples with hydrotalcite coating, sample 2.

(Fig. 4). Cracks are situated locally in the heterogeneous coating (Fig. 4d). The platy hydrotalcite coating can reach as much as 1.4 µm in thickness. A thin and compact layer, composed of Al_2O_3, was developed beneath the highly porous hydrotalcite layer (Fig. 4). Impurity particles from the alloy itself were observed to be incorporated in the upper part of coating, acting as cathodic sites for precipitation during the corrosion tests and therefore decreasing the corrosion resistance ability (Fig. 4c,d).

Coating-corrosion resistance

Data for electrochemical-impedance measurements on coatings with different treatments are shown in Bode plots in Fig. 5. The <1 Hz frequency is relevant to the corrosion reaction, and large impedance values correspond with the high corrosion resistance of the coatings (Mansfeld & Kendig, 1988). The measurements show that the impedance of coatings on Al alloy 6060 increases in the following order: Al substrate without coating < hydrotalcite coating only < hydrotalcite coating + Mg-sealed < hydrotalcite coating + Mg-sealed + Ce immersion + H_2O_2.

During filiform-corrosion testing, corrosion occurs at the interface between the metal and the coating and is manifested in a fibril-like pattern. After 1000 h, the average fibril length (Ø) should not exceed 2 mm and the filiform corrosion factor (F), which is a product of average fibril length and frequency (H), must remain at <0.4 to fulfil the standard DIN EN 3665. In the experiments described, a hydrotalcite coating on Al 6060, sealed by Mg acetate and then dipped in a H_2O_2 + Ce-based solution was proven to impart the greatest resistance to filiform corrosion, followed by hydrotalcite coating on Al 6060 sealed with Mg acetate; hydrotalcite coating with no subsequent treatments demonstrated the greatest level of filiform corrosion

https://doi.org/10.1180/claymin.2015.050.5.03 Published online by Cambridge University Press

during testing (Fig. 6, Table 1). The observation is consistent with the results of the electrochemical impedance measurements on the same treatment of samples.

DISCUSSION

Formation of the coating

When the aluminium plate was exposed to air, a thin, coherent, adhering layer of Al_2O_3 was formed immediately on the surface (Wernick *et al*., 1987); the layer can act as a barrier to prevent further reactions in the coating process. Because of the 'chemical attack' during the pretreatment, however, the alumina layer was supposed to be largely removed, along with the dissolution of substrate. The pickling reactions of Al ions (1 and 2) that occurred when the aluminium surface was exposed to HNO_3 acid during the pretreatment which resulted in the generation of Al^{3+} at anodic areas were:

$$Al_2O_3 + 6H^+ \rightarrow 2Al^{3+} + 3H_2O \quad (1)$$

$$Al + 3H^+ \rightarrow Al^{3+} + 3/2H_2(g) \quad (2)$$

After the treatments with HNO_3 and rinsing with water, the panel was dipped in NaOH solution. Where remnants of the alumina layer were still on the alloy surface, the following reaction took place in the alkali environment:

$$Al_2O_3 + 2OH^- + 3H_2O \rightarrow 2[Al(OH)_4]^-(aq) \quad (3)$$

Where etching by acid had reached the Al substrate, the reaction was:

$$Al(s) + OH^-(aq) + 3H_2O(l) \rightarrow [Al(OH)_4]^-(aq) + 3/2H_2(g) \quad (4)$$

The pickling reaction is essential for the formation of the hydrotalcite coating because it can 'clean' the metal surface chemically, and thus enables the hydrotalcite coating to adhere to the base metal subsequently.

The pretreatment with alkali solution (NaOH) increased the OH^- concentration at the interface between the Al substrate and the spray which carries the coating solution. The ions generated during the pretreatment will combine with external ions from the coating solution, *i.e.* Al^{3+}, Li^+, NO_3^- and OH^-, to precipitate in a supersaturated environment and form Li-Al-NO_3 hydrotalcite on the alloy surface. This compound has a structure similar to that of brucite ($Mg(OH)_2$), where octahedra of Mg^{2+} (6-fold coordinated to OH^-) share edges to form infinite sheets. These sheets are stacked on top of each other and held together by hydrogen bonding. In the case of Li-Al-NO_3 hydrotalcite, Mg^{2+} ions in the octahedra are substituted by trivalent Al^{3+} and univalent Li^+. The net positive charge caused by the substitutions is compensated by interlayer anions, which are located between two brucite-like sheets. The adsorbed water molecules

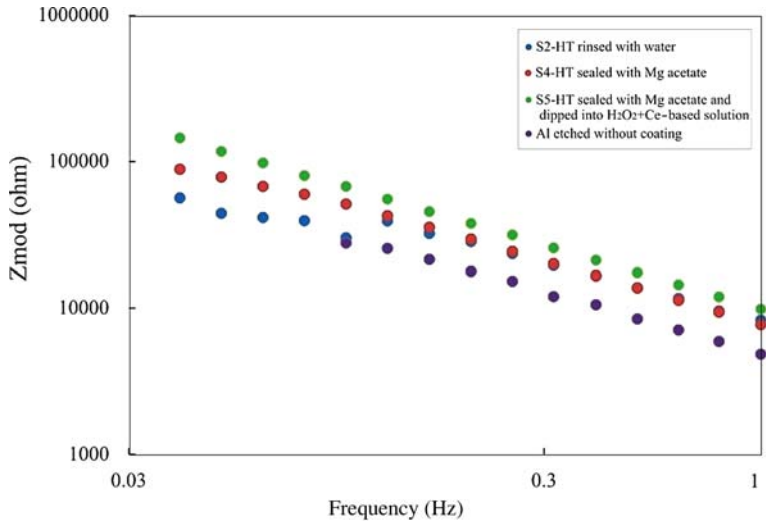

FIG 5. Bode impedance plots for the Al alloy 6060 with hydrotalcite coating.

https://doi.org/10.1180/claymin.2015.050.5.03 Published online by Cambridge University Press

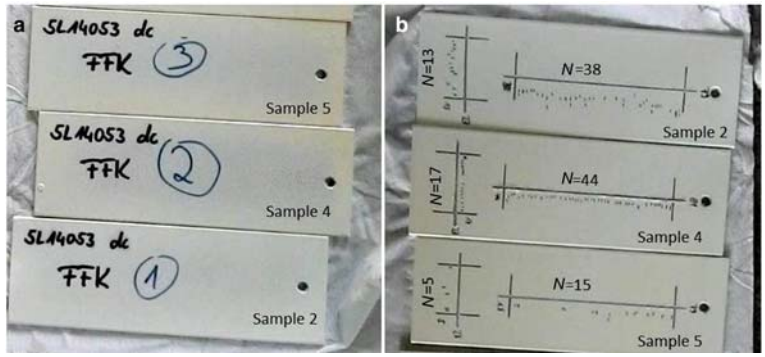

FIG 6. Images of filiform corrosion test of painted samples with coatings: (a) before the test; (b) after 1000 h.

also find a place in the free interlayer space. The sheets containing cations are built as in brucite, where the Al^{3+} and Li^{+} cations occupy randomly the octahedral sites in the close-packed configuration of the OH^{-} ions. These hydroxyls are tied to the NO_3^- groups directly or *via* intermediate H_2O through hydrogen bridges: OH–NO_3–HO or OH–H_2O–NO_3–HO.

However, a multi-layer structure was revealed by the GDOES and the cross-sectional SEM analyses, consisting of the uppermost layer composed of hydrotalcite, as deduced from the acicular crystal shape, and another layer underneath consisting of Al_2O_3, which corresponds to the XRD results. The structural features also suggest that the chemical pretreatment of substrate surface by HNO_3 and NaOH solution in the experiments described are not thorough enough to clear away the Al_2O_3 layer.

Corrosion-resistant mechanism

Compared to NO_3^-, Cl^- is bound preferentially in the interlayer structure of the hydrotalcite crystals (Miyata, 1983). In addition, hydrotalcite shows excellent adsorption ability because of the large surface areas resulting from the laminar structure, which also benefits the adsorption of Cl^- (Frost *et al*., 2008). Other studies have also found the phenomenon of Cl^- adsorption on hydrotalcite films in the coating industry (*e.g.* McMurray & Williams, 2004). Cl^- can typically break down $Al(OH)_3$ units continuously through the

TABLE 1. Parameters for filiform corrosion test for 1000 h on painted samples with coatings.

Sample no.	Fibrial location	Fibrial average length, Ø (mm)	Fibrial maximum length, I_{max} (mm)	Fibrial amounts, N	Fibrial frequency, H	Scratch length, L (mm)	Filiform corrosion factor, F	Sample description
2	Horizontal scratch	2.5	4.7	38	0.48	79	1.20	Hydrotalcite coating
	Vertical scratch	1.5	5.2	13	0.48	27	0.72	
4	Horizontal scratch	0.8	2.4	44	0.54	81	0.43	Hydrotalcite coating sealed with Mg acetate
	Vertical scratch	0.7	1.7	17	0.63	27	0.44	
5	Horizontal scratch	0.9	2.7	15	0.19	79	0.17	Hydrotalcite coating sealed with Mg acetate + $CeNO_3/H_2O_2$
	Vertical scratch	2.1	4.0	5	0.22	23	0.46	

Note: $H = N/L$, $F = Ø \times (N/L)$.

https://doi.org/10.1180/claymin.2015.050.5.03 Published online by Cambridge University Press

replacement of OH^- to form $AlCl_3$. Anion-exchange and adsorption of Cl^- to the crystal structure are supposed to be corrosion-resistant mechanisms for Li-Al-NO_3 hydrotalcite coating to keep the aggressive Cl^- from penetrating the coating layer and attacking the substrate.

Micro-cracks favor the decomposition of coatings by increasing the number of defect spots. These defects can result from mechanical damage, edge alignment or disturbance of the coating. During the filiform-corrosion test, the main culprits were chlorides together with moisture and oxygen which promote the migration of a local anode through the defects at the interface of the coating and the Al alloy, and the corrosion signature is shown as 'fibril development'. During the sealing process, the number of cracks on the hydrotalcite film can be reduced significantly by precipitating new crystals on the Al substrate through the channels provided by the cracks, and therefore a relatively uniform film was developed. In the experiments described, the Al alloy with hydrotalcite film was exposed to a later treatment bath with magnesium acetate ($Mg(C_2H_3O_2)_2$). The Mg^{2+}, OH^- and CO_3^{2-} released from the dissolution of magnesium acetate in the later treatment solution may replace the Li^+ and NO_3^- in Li-Al hydrotalcite to form new crystal phases which include $Mg(OH)_2 \pm$ Mg-Al-CO_3 hydrotalcite, and therefore sealing the cracks and providing a better corrosion-resistance performance of the film (Fig. 5).

After sealing, the coated Al alloy was dipped in Ce(III) solution mixed with hydrogen peroxide (H_2O_2). Ce(IV) species "stored" within the coating enable the self-healing effect (Buchheit *et al*., 2002). The addition of H_2O_2 to Ce(III)-based solution has been demonstrated to accelerate the precipitation of a Ce-conversion coating layer (Hinton & Wilson, 1989).

During the dipping, hydroxyl ions are generated from the reduction of H_2O_2 at cathodic sites (Ardelean *et al*., 2001; Wang *et al*., 2004):

$$H_2O_2(aq) + 2e^- \rightarrow 2OH^-(aq) \quad (5)$$

The OH^- released from reaction 5 will increase the pH values at the interface of the coating layer and dipping solution, which affects significantly the solubility of Ce species in solution. Because most Ce species are more soluble at low pH values (Dabalà *et al*., 2001; Kiyota *et al*., 2011), the increase in pH will precipitate most of the Ce species as hydroxides/oxides on the sealed hydrotalcite coating:

$$Ce^{3+}(aq) + 3OH^-(aq) \rightarrow Ce(OH)_3(s) \quad (6)$$

The strong oxidizing property of H_2O_2 can also transform Ce(III) to Ce(IV) in the solution by forming a complex:

$$2Ce^{3+}(aq) + 3H_2O_2(aq) + 2OH^-(aq) \rightarrow 2Ce(OH)_2^{2+}(aq) \quad (7)$$

and this Ce(IV) complex can react with OH^- to form a Ce oxide film containing mainly Ce(IV):

$$Ce(OH)_2^{2+}(aq) + 2OH^-(aq) \rightarrow CeO_2 \cdot H_2O(s) + H_2O \quad (8)$$

$$Ce(OH)_2^{2+}(aq) + 2OH^-(aq) \rightarrow CeO_2 + 2H_2O \quad (9)$$

Compared to the hydrotalcite coating sealed with Mg acetate, further dipping of the coated alloy in H_2O_2 + Ce(III)-based solution can lead to the deposition of Ce hydroxide/oxide layers, and consequently improve the corrosion-resistance ability (Figs 5, 6).

CONCLUSIONS

Li-Al-NO_3 hydrotalcite conversion coatings were formed on the Al alloy 6060 by exposing the alloy to alkaline lithium salt solutions in a spray system. A well crystallized hydrotalcite-like phase was present in the coating. Sealing with Mg acetate and dipping into H_2O_2 + Ce-based solution of the coated panels can further improve the corrosion resistance. The average coating thickness was ~1000 nm and a multi-layer structure was observed which consists mainly of a porous hydrotalcite top layer and a compact Al_2O_3 layer beneath.

ACKNOWLEDGMENTS

The present study was supported by the Danish National Advanced Technology Foundation. Dan-color is acknowledged for financial and laboratory support.

REFERENCES

Ardelean H., Fiaud C. & Marcus P. (2001) Enhanced corrosion resistance of magnesium and its alloys though the formation of cerium (and aluminium) oxide surface films. *Materials and Corrosion*, **52**, 889–895.

Barisone E., Girard G., Tschopp G., Nelis T., Roske L., De Puydt Y. & Raynaud P. (2011) Glow discharge optical emission spectroscopy: GD-OES, rapid analytical assistance for plasma film deposition. *18th international colloquium on plasma processes (CIP 2011)*.

https://doi.org/10.1180/claymin.2015.050.5.03 Published online by Cambridge University Press

Basile F. & Vaccari A. (2001) Applications of hydrotalcite-type anionic clays (layered double hydroxides) in catalysis. Pp. 285–321 in: *Layered Double Hydroxides: Present and Future* (V. Rives, editor). Nova Publishers, New York.

Brindley G.W. & Kikkawa S. (1980) Thermal behavior of hydrotalcite and of anion-exchanged forms of hydrotalcite. *Clays and Clay Minerals*, **28**, 87–91.

Buchheit R.G. & Guan H. (2004) Formation and characteristics of Al-Zn hydrotalcite coatings on galvanized steel. *Journal of Coatings Technology Research*, **1**, 277–290.

Buchheit R.G., Mamidipally S.B., Schmutz P. & Guan H. (2002) Active corrosion protection in Ce-modified hydrotalcite conversion coatings. *Corrosion*, **58**, 3–14.

Buchheit R.G., Guan H., Mahajanam S. & Wong F. (2003) Active corrosion protection and corrosion sensing in chromate-free organic coatings. *Progress in Organic Coatings*, **47**, 174–182.

Cavani F., Trifirò F. & Vaccari A. (1991) Hydrotalcite-type anionic clays: Preparation, properties and applications. *Catalysis Today*, **11**, 173–301.

Chen J., Song Y., Shan D. & Han E.H. (2012) Study of the in situ growth mechanism of Mg-Al hydrotalcite conversion film on AZ31 magnesium alloy. *Corrosion Science*, **63**, 148–158.

Dabalà M., Armelao L., Buchberger A. & Calliari I. (2001) Cerium-based conversion layers on aluminium alloys. *Applied Surface Science*, **172**, 312–322.

Frost R.L., Bahfenne S., Graham J. & Reddy B.J. (2008) The structure of selected magnesium carbonate minerals – a near infrared and mid-infrared spectroscopic study. *Polyhedron*, **27**, 2069–2076.

Hinton B.R.W. & Wilson L. (1989) The corrosion inhibition of zinc with cerous chloride. *Corrosion Science*, **29**, 967–975.

Kannan S. (2006) Catalytic applications of hydrotalcite-like materials and their derived forms. *Catalysis Surveys from Asia*, **10**, 117–137.

Kiyota S., Valdez V., Stoytcheva M., Zlatev R. & Bastidas J. M. (2011) Anticorrosion behavior of conversion coatings obtained from unbuffered cerium salts solutions on AA6061-T6. *Journal of Rare Earth*, **29**, 961–968.

Lin J.K. & Uan J.Y. (2009) Formation of Mg, Al-hydrotalcite conversion coating on Mg alloy in aqueous HCO_3^-/CO_3^{2-} and corresponding protection against corrosion by the coating. *Corrosion Science*, **51**, 1181–1188.

Lin J.K., Hsia C.L. & Uan J.Y. (2007) Characterization of Mg, Al-hydrotalcite conversion film on Mg alloy and Cl^- and anion-exchangeability of the film in a corrosive environment. *Scripta Materialia*, **56**, 927–930.

Mansfeld F. & Kendig M.W. (1988) Evaluation of anodized aluminum surfaces with electrochemical impedance spectroscopy. *Journal of the Electrochemistry Society*, **135**, 828.

McMurray H.N. & Williams G. (2004) Inhibition of filiform corrosion on organic-coated aluminum alloy by hydrotalcite-like anion-exchange pigments. *Corrosion*, **60**, 219–228.

Miyata S. (1983) Anion-exchange properties of hydrotalcite-like compounds. *Clays and Clay Minerals*, **31**, 305–311.

Orthman J., Zhu H.Y. & Lu G.Q. (2003) Use of anion clay hydrotalcite to remove coloured organics from aqueous solutions. *Separation and Purification Technology*, **31**, 53–59.

Reichle W.T. (1986) Synthesis of anionic clay minerals (mixed metal hydroxides, hydrotalcite). *Solid State Ionics*, **22**, 135–141.

Ruggeri R.T. & Beck T.R. (1983) An analysis of mass transfer in filiform corrosion. *Corrosion*, **39**, 452–465.

Syu J.H., Uan J.Y., Lin M.C. & Lin Z.Y. (2013) Optically transparent Li–Al–CO_3 layered double hydroxide thin films on an AZ31 Mg alloy formed by electrochemical deposition and their corrosion resistance in a dilute chloride environment. *Corrosion Science*, **68**, 238–248.

Taylor R.M. (1984) The rapid formation of crystalline double hydroxy salts and other compounds by controlled hydrolysis. *Clay Minerals*, **19**, 591–603.

Valdez B., Kiyota S., Stoytcheva M., Zlatev R. & Bastidas J.M. (2014) Cerium-based conversion coatings to improve the corrosion resistance of aluminium alloy 6061-T6. *Corrosion Science*, **87**, 141–149.

Valente J.S., Rodriguez-Gattorno G., Valle-Orta M. & Torres-Garcia E. (2012) Thermal decomposition kinetics of MgAl layered double hydroxides. *Materials Chemistry and Physics*, **133**, 621–629.

Wang C., Jiang F. & Wang F. (2004) Cerium chemical conversion for aluminium alloy 2024-T3 and its corrosion resistance. *Corrosion*, **60**, 237–243.

Wang J., Li D., Yu X., Jing X., Zhang M. & Jiang Z. (2010) Hydrotalcite conversion coating on Mg alloy and its corrosion resistance. *Journal of Alloys and Compounds*, **494**, 271–274.

Wernick S., Pinner R. & Sheasby P.G. (1987) *The Surface Treatment and Finishing of Aluminum and its Alloys.* Finishing Publications Ltd., Teddington, Middlesex, UK.

Williams G. & McMurray H.N. (2003) Anion-exchange inhibition of filiform corrosion on organic coated AA2024-T3 aluminum alloy by hydrotalcite-like pigments. *Electrochemical and Solid-State Letters*, **6**, B9–B11.

Williams G. & McMurray H.N. (2004) Inhibition of filiform corrosion on polymer coated AA2024-T3 by hydrotalcite-like pigments incorporating organic anions. *Electrochemical and Solid-State Letters*, **7**, B13–B15.

Zhang W. & Buchheit R.G. (2002) Hydrotalcite coating formation on Al-Cu-Mg alloys from oxidizing bath chemistries. *Corrosion*, **58**, 591–600.

https://doi.org/10.1180/claymin.2015.050.5.03 Published online by Cambridge University Press